3D QSAR Studies on Substituted Benzimidazole Derivatives as Angiotensin II-AT₁ Receptor Antagonist

Vivek K. Vyas[*,1], Manjunath Ghate[1], Chetan Chintha[1] and Paresh Patel[2]

[1]*Department of Pharmaceutical Chemistry, Institute of Pharmacy, Nirma University, Ahmedabad 382 481, Gujarat, India*

[2]*Department of Pharmaceutical Chemistry, L.J. Institute of Pharmacy, Ahmedabad 382 210, Gujarat, India*

Abstract: This study investigated 3D quantitative structure–activity relationships (QSAR) for a range of substituted benzimidazole derivatives as AngII-AT₁ receptor antagonists by comparative molecular field analysis (CoMFA) and comparative molecular similarity indices (CoMSIA). The alignment strategy was used for these compounds by means of Distill function defined in SYBYL X 1.2. The best CoMFA and CoMSIA models were obtained for the training set compounds was statistically significant with leave-one-out (LOO) validation correlation coefficient (q^2) of 0.613 and 0.622, cross validated coefficient (r^2_{cv}) of 0.617 and 0.607, respectively and conventional coefficient (r^2_{ncv}) of 0.886 and 0.859, respectively. Both the models were validated by a test set of 18 compounds giving satisfactory predicted correlation coefficient (r^2_{pred}) of 0.714 and 0.549 for CoMFA and CoMSIA models, respectively. Generated 3D QSAR models were used for the prediction of pIC₅₀ of an external dataset of 10 compounds for predictive validation, which gave conventional r^2 of 0.893 for CoMFA model, and 0.774 for CoMSIA model. We identified some key features in substituted benzimidazole derivatives, such as the importance of lipophilicity and H-bonding at 2- and 5, 6, 7- position of benzimidazole ring, respectively, for good antagonistic activity. CoMFA and CoMSIA models generated in this work provide useful information for the design of new compounds and helped in prediction of antagonistic activity.

Keywords: 3D QSAR, AngII, ARBs, CoMFA, CoMSIA, Substituted benzimidazole derivatives.

1. INTRODUCTION

The renin-angiotensin system (RAS) is a complex and highly regulated pathway, which is known to play an important role in the regulation of blood volume, electrolyte balance and arterial blood pressure for management of hypertension [1, 2]. The RAS cascade begins with the biosynthesis of rennin enzyme by the juxtaglomerular cells (JG) of the renal glomerulus [3]. Renin regulates the initial, rate-limiting step of the RAS by cleaving the N-terminal portion of a large molecular weight globulin, angiotensinogen, to form a biologically inert decapeptide AngI, which in turn is hydrolyzed by angiotensin-converting enzyme (ACE), and removes the C-terminal dipeptide to form the octapeptide AngII [4, 5]. AngII is a primary active product of the RAS and induced many physiological and pathophysiological actions. AngII is a potent vasoconstrictor, which regulates blood pressure homeostasis, fluid volume and electrolyte balance [6, 7]. AngII exhibits its effects by binding with specific angiotensin receptors in plasma membrane [8]. Angiotensin receptors (type 1 (AT₁) and type 2 (AT₂) are 7-transmembrane spanning receptors that belong to the G protein-coupled receptor (GPCRs) family. AngII binds with high affinity to AT₁ and AT₂ angiotensin receptors. Physiological actions of AngII on cardiovascular, neuronal, renal, hepatic, endocrine and other target cells are mainly due to interaction with AT₁ receptor [9-11]. AT₁ receptor mediates most of the established physiological and pathophysiological effects of AngII. These include increased blood pressure, increased cardiac contractility, vasoconstriction, renal tubular sodium reabsorption (fluid balance), vascular and cardiac hypertrophy, inhibition of renin release and stimulation of aldosterone synthesis and secretion (zona glomerulosa) [12-14]. AngII mediates cell growth and proliferation, inflammatory responses, and oxidative stress due to activation of the AT₁ receptor [15]. Inhibition of RAS is an effective way to control pathogenesis of cardiovascular and renal disorders (Fig. **1**).

Earlier it was thought that inhibition of either renin or ACE would results in a decreased formation of AngII, so renin inhibitors and angiotensin converting enzyme inhibitors (ACEIs) were developed as RAS blocking agents for the treatment of hypertension. Renin inhibitors were challenged by poor pharmacokinetic properties, such as low oral bioavailability [15]. ACEIs contribute side-effects like cough [16] and angioedema [17] due to inhibition of inactivation of bradykinin. Thus, with the discovery of different angiotensin receptors, a new class of compounds known as AngII receptor blockers (ARBs) are developed for the treatment of hypertension. ARBs specifically antagonize actions of AngII at the AT₁ receptor rather than inhibiting its synthesis. Development of nonpeptide, selective ARBs began in the 1990s with the discovery of losartan [18]. A number of new oral, nonpeptide ARBs similar to losartan were developed based upon replacement of imidazole ring of losartan with other heterocyclic ring systems (benzimida-

*Address correspondence to this author at the Department of Pharmaceutical Chemistry, Institute of Pharmacy, Nirma University, S.G. Highway, Charodi, Ahmedabad 382 481, Gujarat, India; Tel: +91 9624931060; Fax: +91 2717 241916;
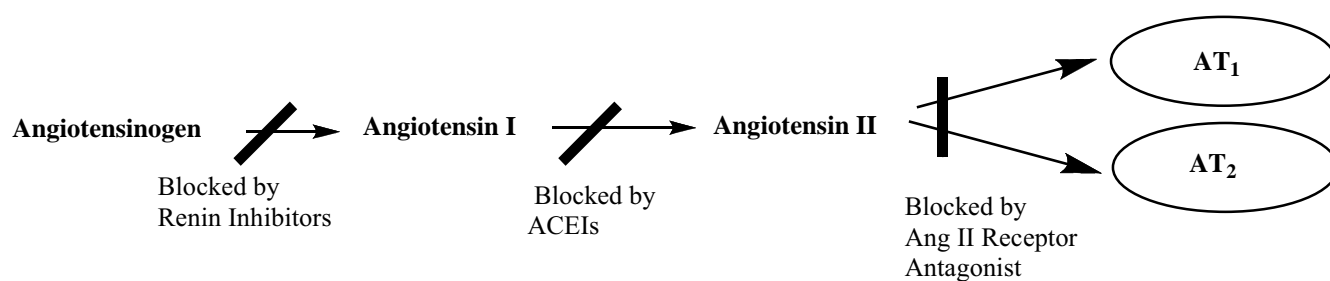E-mails: vicky_1744@yahoo.com, vivekvyas@nirmauni.ac.in

Angiotensinogen → Angiotensin I → Angiotensin II → AT₁ / AT₂

Fig. (1). Block of renin angiotensin system (RAS) at various points.

zole), which appears to be effective antihypertensive agents both in animal studies and in preliminary clinical trials. Many different substitutions, especially at 2- and 6- position of benzimidazole nucleus were evaluated for their affinity, potency, and antihypertensive effects, which led to the development of potent, orally active, competitive nonpeptide ARBs. Keiji Kubo and Colleagues at Takeda Chemical Industries of Osaka in Japan [19] were the first to discover a series of 2-substituted benzimidazole bearing biphenyl moiety, which led to the development of candesartan (**56b**) (Table **1**). Uwe J. Ries [20] and Colleagues disclosed a series of 6-substituted benzimidazole, among them telmisartan (6-(benzimidazol-2-yl)benzimidazole) was found as potent ARB. Substituted benzimidazole as ARBs appears to provide an opportunity as better therapeutic agents for treatment of hypertension and related cardiovascular disorders. We had published a review listing many substituted benzimidazole as ARBs and described advances for targeting AT₁ receptor [21]. Many different QSAR studies were performed for ACE-inhibitory activity. Sagardia, *et al.* [22] established QSAR models with 263 ACE inhibitory peptides using 38 physicochemical descriptors. He, *et al.* [23] developed QSAR model of ACE inhibitory peptides with an artificial neural network (ANN) approach. Shu, *et al.* [24] applied P-scale for the study of QSARs models on three ACE inhibitory peptides datasets (58 dipeptides, 55 tripeptides, and 50 tetrapeptides). Wang, *et al.* [25] derived a novel set of descriptors G-scale, and applied them to study on QSARs of nine peptide datasets of ACE-inhibitor oligopeptides. Ponce, *et al.* [26] developed LDA-QSAR model for ACE-inhibitory activity of perindoprilate's sigma-stereoisomers combinatorial library and predicted sigma-receptor antagonist activities. Gupta [27], reviewed QSAR study of various classes of antihypertensive agent and suggested an overall picture of the mode of action of each class of antihypertensive drugs. Diaz, *et al.* [28] modeled the ACE inhibitory activity of perindoprilate's sigma-stereoisomer combinatorial library using MARCH-INSIDE methodology to codify chemical structure information for chiral drugs. Castillo-Garit, *et al.* [29, 30] evaluated the effectiveness of non-stochastic and stochastic 2D bilinear indices and bond-based 3D-chiral linear indices to codify chemical structure information for chiral drugs as a novel approach and modeled the ACE inhibitory activity of perindoprilate's sigma-stereoisomers combinatorial library. QSAR study [31] was performed in order to gain insight into the structural requirement of 4, 5, 6 and 7 substituted benzimidazoles as AngII receptor antagonist. Another QSAR studies [32, 33] were performed to demonstrated the importance of geometrical, structural and shape descriptors for governing AngII antagonistic activity. Sharma, *et al.* perfomed 2D and 3D QSAR studies on 5-carboxyl-imidazolyl-biphenyl-sulfonylureas [34], substituted quinolines derivatives [35], substituted benzimidazoles [36], substituted 5-(biphenyl-4-ylmethyl)-pyrazoles derivatives [37], 2,3,5-trisubstituted-4,5-dihydro-4-oxo-3*H*-imidazo[4,5-*c*]-pyridine derivatives [38], aryltriazolinone derivatives [39] and 3-substituted-6-butyl-1,2-dihydropyridin-2-ones [40] as AngII receptor antagonists. We performed in the past a 2D QSAR study on a series of substituted benzimidazole derivatives using WHIM descriptors [41] and on a series of 2-alkyl-4-(biphenylmethoxy)quinolines [42] as ARBs. Though many different QSAR studies were performed in the past and in recent time on different chemical compounds as ARBs, to the best of our knowledge no 3D QSAR investigations for substituted benzimidazole derivatives were reported to date with such kind of methods (CoMFA and CoMSIA). As a continuation of our research on ARBs, this study aims to build the predictive 3D QSAR models using CoMFA and CoMSIA methods, and using these models to find the correlation between the structure of substituted benzimidazole derivatives and activity to design more potent and selective ARBs.

CoMFA is a versatile and powerful tool in rational drug design, it calculates steric and electrostatic fields surrounding the molecules and correlating the differences in these fields to antagonistic activity [43, 44]. CoMFA model can be used for the design and prediction of binding affinities of ARBs. In CoMSIA, similarity indices are calculated at regularly placed grid points for the aligned molecules. CoMSIA calculates other molecular descriptors like hydrophobic fields and hydrogen-bond donor and acceptor fields [45]. The contour maps of the CoMFA/CoMSIA fields describe the 'favorable' and 'unfavorable' region of interest surrounding the ligands to the target property. This paper presents the first study using 3D QSAR (CoMFA and CoMSIA) computational approach dealing with substituted benzimidazole derivatives as ARBs.

2. MATERIALS AND METHODS

2.1. Data Preparation

The AngII-AT₁ receptor antagonistic activity data of substituted benzimidazole derivatives were collected from the published literature [19, 46, 47] consisting of 92 compounds, which consisted of 2-butyl-4,5,6,7-substituted-biphenyl-4-yl-methyl-bennzimidazoles (33 compounds) [46],

Table 1.   **Structures and Activity of Substituted Benzimida-zole Derivatives as ARBs**
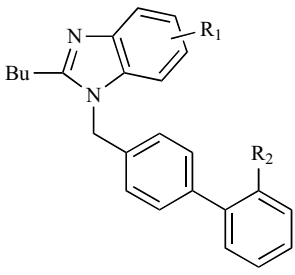
(a)

Compound	R_1	R_2	IC_{50}^{a} $(10^{-7}\,M)$	pIC_{50}^{b}
1a[t]	H	Tetrazole	9	6.046
2a	5-OMe	Tetrazole	9.1	6.041
3a	6-OMe	Tetrazole	11	5.959
4a	5-Cl	Tetrazole	15	5.824
5a	6-Cl	Tetrazole	31	5.509
6a	7-OMe	Tetrazole	28	5.553
7a[t]	4-CO_2Me	Tetrazole	72	5.143
8a	5-CO_2Me	Tetrazole	7.4	6.131
9a	6-CO_2Me	Tetrazole	4.4	6.357
10a	7-CO_2Me	Tetrazole	3.2	6.495
11a	5-Me, 7-CO_2Me	Tetrazole	8.7	6.060
12a	5-Cl, 7-CO_2Me	Tetrazole	4.4	6.357
13a	6-Me,7-CO_2Et	Tetrazole	9.1	6.041
14a[t]	4-$CONH_2$	Tetrazole	130	4.886
15a	7-CO_2Et	Tetrazole	14	5.854
16a	7-COOBu	Tetrazole	12	5.921
17a	5-COOH	Tetrazole	55	5.260
18a	6-COOH	Tetrazole	90	5.046
19a[t]	7-COOH	Tetrazole	5.5	6.260
20a	5-Me, 7-COOH	Tetrazole	13	5.886
21a	5-Cl, 7-COOH	Tetrazole	11	5.959
22a	6-Me, 7-COOH	Tetrazole	3.4	6.469
23a	H	COOH	11	5.959
24a	7-COOH	COOH	6.6	6.180
25a	7-COOH	1-Me- tetrazole	34	5.469
26a[t]	7-CONH*i*-Pr	Tetrazole	5.4	6.268
27a	7-CH_2OH	Tetrazole	4.5	6.347
28a	7-CH_2OMe	Tetrazole	6	6.222
29a[t]	7-CH_2NMe_2	Tetrazole	24	5.620
30a	7-Me	Tetrazole	3.3	6.481
31a	7-CH_2COOEt	Tetrazole	2.5	6.602
32a	7-OH	Tetrazole	11	5.959
33a	7-CH_2COOH	Tetrazole	26	5.585

(Table 1) contd…...
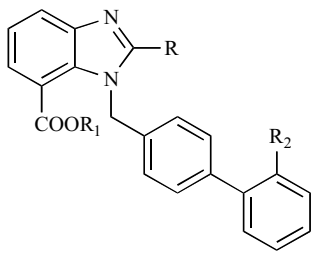
(b)

Compound	R	R_1	R_2	IC_{50}^{a} $(10^{-7}\,M)$	pIC_{50}^{b}
34b	EtO	H	COOH	1.9	6.721
35b	MeO	Me	Tetrazole	4.9	6.310
36b[t]	EtO	Me	Tetrazole	0.66	7.180
37b	PrO	Et	Tetrazole	10	6.000
38b	$CH_2=CHCH_2O$	Me	Tetrazole	8.5	6.071
39b	EtS	Me	Tetrazole	4.4	6.357
40b	Me	Me	Tetrazole	1.9	6.721
41b	Et	H	Tetrazole	0.46	7.337
42b	Pr	H	Tetrazole	1.7	6.770
43b[t]	*i*-Pr	H	Tetrazole	0.82	7.086
44b	*c*-Pr	H	Tetrazole	0.84	7.076
45b	*s*-Bu	H	Tetrazole	39	5.409
46b	*i*-Bu	H	Tetrazole	32	5.495
47b	Pentyl	H	Tetrazole	5.6	6.252
48b	$MeOCH_2$	H	Tetrazole	2.5	6.602
49b	$EtOCH_2$	H	Tetrazole	4.4	6.357
50b	$MeSCH_2$	H	Tetrazole	1.5	6.824
51b[t]	$EtSCH_2$	H	Tetrazole	3.0	6.523
52b	$MeOCH_2CH_2$	H	Tetrazole	5.8	6.237
53b	$MeSCH_2CH_2$	H	Tetrazole	6.2	6.208
54b[t]	$MeNHCH_2$	H	Tetrazole	8.0	6.097
55b	MeO	H	Tetrazole	0.32	7.495
56b	EtO	H	Tetrazole	1.1	6.959
57b	PrO	H	Tetrazole	1.9	6.721
58b	CF_3CH_2O	H	Tetrazole	5.8	6.237
59b[t]	MeNH	H	Tetrazole	1.7	6.770
60b	EtNH	H	Tetrazole	0.62	7.208
61b	PrNH	H	Tetrazole	0.39	7.409
62b	BuNH	H	Tetrazole	6.5	6.187
63b	MeS	H	Tetrazole	1.2	6.921
64b	EtS	H	Tetrazole	1.7	6.770
65b[t]	PrS	H	Tetrazole	1.2	6.921
66b	Bu	H	Tetrazole	5.5	6.260

(Table 1) contd…...

(c)

Compound	R₁	R₂	R₃	IC$_{50}$^{a} (10^{-7} M)	pIC$_{50}$^{b}
67c	EtO	CH₃	(1,2,4-thiadiazol-5(4H)-one)	7.5	6.125
68c^t	EtS	H		4.7	6.013
69c	MeNH	H		5.4	6.268
70c	EtNH	H		1.3	6.886
71c	Et	H		3.4	6.469
72c	Pr	H		3.9	6.409
73c^t	Bu	H		7.6	6.119
74c	MeS	H		10	6.000
75c	EtS	H		6.9	6.161
76c^t	EtO	CH₃		4.6	6.337
77c	Bu	CH₃		10	6.000
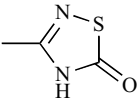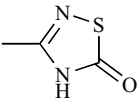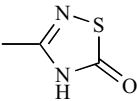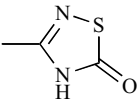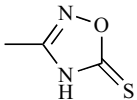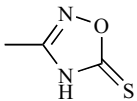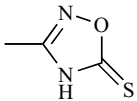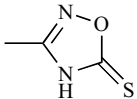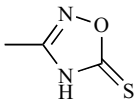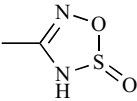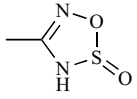
(Table 1) contd…...

Compound	R₁	R₂	R₃	IC$_{50}$^{a} (10^{-7} M)	pIC$_{50}$^{b}
78c	Me	H		9.7	6.013
79c	EtO	CH₃		4.4	6.357
80c	Bu	H		6.2	6.208
81c^t	EtO	H		4.2	6.377
82c	Bu	CH₃		3.2	6.495
83c	EtO	CH₃		0.66	7.180
84c	Bu	H		5.5	6.260
85c	EtO	H		1.1	6.959
86c	Et	H		0.69	7.161
87c	Pr	H		3.6	6.444
88c^t	Bu	H		7.2	6.143
89c	Meo	H		3.6	6.444
90c	EtO	H		2.5	6.602
91c^t	PrO	H		9.2	6.036
92c	MeS	H		5.0	6.301
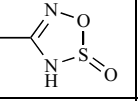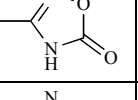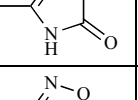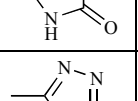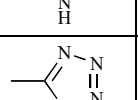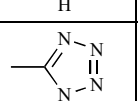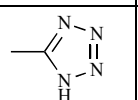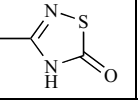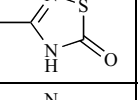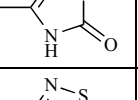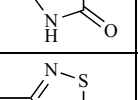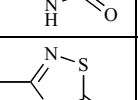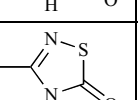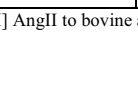
^{a} Inhibition of specific binding of [^{125}I] AngII to bovine adrenal cortex (IC$_{50}$ X 10^{-7} M).
^{b} Negative logarithm of IC$_{50}$ (pIC$_{50}$).
^{t} Test set.

2-substituted-benzimidazole carboxylic acids (33 compounds) [19] and 2-substituted-benzimidazole-7-carboxylic acids bearing novel tetrazole bioisosteres (26 compounds) [47]. In the literature [19, 46, 47] experimental IC_{50} values were evaluated by inhibition of specific binding of [^{125}I] AngII to bovine adrenal cortex, which employed similar experimental conditions and procedures. The IC_{50} values were converted pIC_{50} and subsequently used as dependent variable for 3D QSAR study (Table **1**). The pIC_{50} value of the molecules under the study spanned a wide range from 4 to 7.5.

2.2. Computational details

3D QSAR study, calculations and visualizations for CoMFA and CoMSIA analysis were performed using SYBYL X 1.2 software from Tripos Inc., St. Louis, MO, USA [48]. Compound **55b** was selected as template molecule because of its high antagonistic activity. The structures of all other compounds were constructed from the template molecule by using the "SKETCH" option function in SYBYL, and partial atomic charges were calculated by the Gasteiger Huckel method and energy minimizations were performed using the Tripos force field [49] with a distance-dependent dielectric and the Powell conjugate gradient algorithm. The minimum gradient difference of 0.05 kcal/mol Å was set as a convergence criterion [50].

2.3. Construction of Training and Test Sets Using Hierarchical Cluster Analyses

To construct training and test set compounds HCA was performed. HCA aims to divide a data set of all the compounds into clusters. Once a set of molecules has been clustered then a representative subset can be chosen simply by selecting one (or more) compounds from each cluster, therefore the structural diversity and activity range of the test set are comparable with the training set. A data set of 92 molecules was divided into training set (74 compounds) and test set (18 compounds) using HCA. HCA is an approach to select training and test sets based on structural similarities; it attempts to find groupings within the data set. Hierarchical clustering method starts at the bottom of the dendogram (all compounds in separate clusters) and proceed by merging the most similar clusters together in an iterative manner. Thus, in the first step the closest two compounds are merged into a single cluster. In the next step, the closest two clusters are merged and so on. The analysis moves from the bottom of the dendrogram to the top, with each node at the bottom representing a row in the table, and the central branch at the top representing entire table. Notice however that left-to right order of nodes at the bottom of the dendrogram is determined only by the requirement that branches may not cross, and is thus incidentally related to the row order in original table. The lengths of the vertical lines in the dendrogram provide qualitative information about separation, or linkage distance, between various clusters. Clusters represented by long unbranched strands are strongly separated from other clusters [51]. The ratio of compounds for the training and test set was chosen using CoMFA field and pIC_{50} values. A total number of 18 clusters were derived from the data set. One compound from each cluster was arbitrarily selected for a test set.

2.4. Alignment

Rigid body alignment of molecules in a Mol2 database was performed using maximum common substructure (MCS) defined by Distill function. Compound **55b** (Fig. **2**) was used as a template and all other compounds were aligned on the basis of the common structure. MCS represents a common core of all the structures used for the alignment. Distill generates MCS on the basic of a group of connected atoms common to a set of structures used for the alignment. A rigid alignment attempts to align molecules in a database to a template molecule on a common backbone or core (MCS). This core (benzimidazole ring) was produced by Distill.
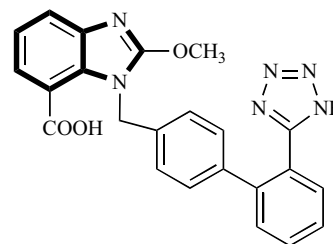
Fig. (2). Structure of the template compound 55b, maximum common substructure (MCS) benzimidazole ring is in bold face.

2.5. CoMFA Model

CoMFA steric and electrostatic interaction fields of each molecule were calculated on a 3D cubic lattice with grid spacing of 2 Å in all the Cartesian directions. CoMFA fields were calculated using the QSAR module of SYBYL. CoMFA descriptors were calculated using sp^3 carbon probe atom with a van der Waals radius of 1.52 Å and a charge of + 1.0 to generate steric (Lennard Jones 6-12 potential) field energies and electrostatic (Coulombic potential) fields with a distance-dependent dielectric at each lattice point. The SYBYL default energy cutoff of 30 kcal/mol was set for both steric and electrostatic fields. In order to reduce noise and improve efficiency, column filtering (minimum sigma) was set to 2.0 kcal/mol.

2.6. CoMSIA Model

CoMSIA similarity index descriptors were derived using the same lattice box as that of CoMFA calculations with a grid spacing of 2 Å employing a C +1 probe atom with a radius of 1.0 Å as implemented in SYBYL. CoMSIA not only computes the steric and electrostatic fields, but also calculates hydrophobic, hydrogen-bond donor (HBD), and hydrogen-bond acceptor (HBA) fields. For the distance dependence between the probe atom and the molecule atoms a Gaussian function was used. Because of the different shape of the Gaussian function, the similarity indices were calculated at all grid points, both inside and outside the molecular surface.

2.7. Partial Least Square (PLS) Analysis

CoMFA and CoMSIA models were derived using PLS regression analysis. Calculated CoMFA and CoMSIA descriptors were used as independent variables and AngII-

AT_1 receptor antagonist activity (pIC_{50}) used as dependent variables in the PLS analysis. PLS analysis was performed using the leave-one-out (LOO) and cross-validation (CV) methods for 3D QSAR analysis, which gives q^2 and r^2_{cv}, respectively as a statistical index of predictive power. In leave-one-out (LOO) validation method, one compound is left out as the testing compound and the rest of the data is used as the training set in PLS analysis. The model was built using the training set and pIC_{50} value and predicted value of testing compound (left out) was determined, which gives q^2. To calculate q^2 following equation was used.

$$q^2 = 1 - \Sigma \, (Y_{pred} - Y_{act})^2 / \Sigma \, (Y_{act} - Y_{mean})$$

Y_{pred}, Y_{act} and Y_{mean} are predicted, actual and mean values of the pIC_{50}, respectively. $\Sigma \, (Y_{pred} - Y_{act})^2$ is a predictive residual error sum of squares (PRESS). The non cross-validated models were assessed by the conventional correlation coefficient (r^2_{ncv}), standard error of estimation (SEE) and F values. A 100-cycle bootstrap analysis was performed to assess the statistical confidence of the derived models. The mean correlation coefficient is represented as bootstrap r^2 (r^2_{boot}). The PLS analysis was then repeated with no validation using the optimum number of components to generate CoMFA and CoMSIA models [52,53].

2.8 Predictive r^2

The predictive r^2 (r^2_{pred}) was based only on a test set molecules (18 compounds), which were not included in the model generation study, and is defined as r^2_{pred} = SD-PRESS/SD where, SD is the sum of the squared deviations between the antagonistic activity of molecules in a test set and the mean antagonistic activity of a training set molecules, and PRESS is the sum of squared deviations between predicted and actual activity values for every molecule in a test set.

2.9. Predictive Validation

The generated 3D QSAR models (CoMFA and CoMSIA) were further validated by prediction of activity using an external data set of 10 different substituted benzimidazole compounds as AngII receptor antagonists [20]. Benzimidazole substituted compounds were aligned with the main data set in the working spread sheet of QSAR modelling.

2.10. Analysis of Residuals

Training set was initially checked for outliers in 3D QSAR analysis. Generally, if the residual of a compound between experimental and predicted pIC_{50} values is greater than 1 logarithm unit, compound is considered as outlier. Examination of the residuals from cross-validated predictions (Table **2**) indicated that there is no outlier in 3D QSAR models.

3. RESULTS AND DISCUSSION

3.1. Results of the CoMFA study

The statistical parameters of standard CoMFA models constructed with steric and electrostatic fields are given in

Table 2. Experimental and Predicted pIC_{50} with Residuals of Training and Test Sets Using CoMFA and CoMSIA Models

Compound	pIC_{50}	CoMFA		CoMSIA	
		Predicted pIC_{50}	Residual	Predicted pIC_{50}	Residual
1a[t]	6.046	5.623	0.423	5.582	0.464
2a	6.041	6.395	-0.354	5.781	0.260
3a	5.959	6.061	-0.102	5.953	0.006
4a	5.824	5.693	0.131	5.627	0.197
5a	5.509	5.599	-0.090	5.598	-0.089
6a	5.553	5.684	-0.131	5.412	0.141
7a[t]	5.143	5.971	-0.828	5.241	-0.098
8a	6.131	6.219	-0.088	5.959	0.172
9a	6.357	6.171	0.186	6.113	0.244
10a	6.495	6.366	0.129	6.456	0.039
11a	6.060	6.107	-0.047	6.256	-0.196
12a	6.357	6.328	0.029	6.316	0.041
13a	6.041	6.071	-0.030	6.046	-0.005
14a[t]	4.886	5.311	-0.425	4.805	0.081
15a	5.854	6.075	-0.221	6.088	-0.234
16a	5.921	6.027	-0.106	6.428	-0.507
17a	5.260	5.520	-0.260	5.271	-0.011
18a	5.046	5.281	-0.235	5.020	0.026
19a[t]	6.260	6.107	0.153	6.430	-0.170
20a	5.886	5.966	-0.080	5.947	-0.061
21a	5.959	6.224	-0.265	6.102	-0.143
22a	6.469	6.387	0.082	6.436	0.033
23a	5.959	6.014	-0.055	5.998	-0.039
24a	6.180	5.985	0.195	6.020	0.160
25a	5.469	5.661	-0.192	5.498	-0.029
26a[t]	6.268	6.738	-0.470	6.659	-0.391
27a	6.347	6.368	-0.021	6.343	0.004
28a	6.222	6.281	-0.059	6.204	0.018
29a[t]	5.620	5.296	0.324	5.496	0.124
30a	6.481	6.413	0.068	6.431	0.050
31a	6.602	6.628	-0.026	6.435	0.167
32a	5.959	6.304	-0.345	6.013	-0.054
33a	5.585	5.825	-0.240	5.692	-0.107
34b	6.721	6.618	0.103	6.741	-0.020
35b	6.310	6.312	-0.002	6.386	-0.076
36b[t]	7.180	7.328	-0.148	7.449	-0.269
37b	6.000	6.016	-0.016	6.096	-0.096
38b	6.071	5.965	0.106	6.139	-0.068
39b	6.357	6.319	0.038	6.399	-0.042
40b	6.721	6.922	-0.201	6.554	0.167

(Table 2) contd…..

Compound	pIC$_{50}$	CoMFA		CoMSIA	
		Predicted pIC$_{50}$	Residual	Predicted pIC$_{50}$	Residual
41b	7.337	7.156	0.181	7.311	0.026
42b	6.770	6.473	0.297	6.574	0.196
43b^t	7.086	7.259	-0.173	7.322	-0.236
44b	7.076	6.951	0.125	6.950	0.126
45b	5.409	5.586	-0.177	5.639	-0.230
46b	5.495	5.586	-0.091	5.639	-0.144
47b	6.252	6.251	0.001	6.269	-0.017
48b	6.602	6.687	-0.085	6.581	0.021
49b	6.357	6.078	0.279	6.310	0.047
50b	6.824	6.896	-0.072	6.647	0.177
51b^t	6.523	6.501	0.022	6.774	-0.251
52b	6.237	6.240	-0.003	6.299	-0.062
53b	6.208	6.190	0.018	6.251	-0.043
54b^t	6.097	6.100	-0.003	6.120	-0.023
55b	7.495	7.475	0.020	7.509	-0.014
56b	6.959	7.155	-0.196	6.890	0.069
57b	6.721	6.669	0.052	6.791	-0.070
58b	6.237	6.379	-0.142	6.218	0.019
59b^t	6.770	7.407	-0.637	6.685	0.085
60b	7.208	7.165	0.043	7.216	-0.008
61b	7.409	7.494	-0.085	7.513	-0.104
62b	6.187	6.438	-0.251	6.209	-0.022
63b	6.921	7.184	-0.263	6.924	-0.003
64b	6.770	6.861	-0.091	6.971	-0.201
65b^t	6.921	6.633	0.288	6.979	-0.058
66b	6.260	6.272	-0.012	6.294	-0.034
67c	6.125	6.223	-0.098	6.062	0.063
68c^t	6.013	6.391	-0.378	6.048	-0.035
69c	6.268	5.985	0.283	6.522	-0.254
70c	6.886	6.839	0.047	6.747	0.139
71c	6.469	6.468	0.001	6.250	0.219
72c	6.409	6.369	0.040	6.217	0.192
73c^t	6.119	6.319	-0.200	6.171	-0.052
74c	6.000	5.890	0.110	6.008	-0.008
75c	6.161	5.932	0.229	6.296	-0.135
76c^t	6.337	6.425	-0.088	6.867	-0.530
77c	6.000	6.121	-0.121	6.076	-0.076
78c	6.013	5.838	0.175	6.151	-0.138
79c	6.357	6.395	-0.038	6.555	-0.198
80c	6.208	6.351	-0.143	6.286	-0.078
81c^t	6.377	6.273	0.104	6.707	-0.330

(Table 2) contd…..

Compound	pIC$_{50}$	CoMFA		CoMSIA	
		Predicted pIC$_{50}$	Residual	Predicted pIC$_{50}$	Residual
82c	6.495	6.410	0.085	6.406	0.089
83c	7.180	6.994	0.186	7.243	-0.063
84c	6.260	6.530	-0.270	6.441	-0.181
85c	6.959	6.609	0.350	6.924	0.035
86c	7.161	6.925	0.236	7.111	0.050
87c	6.444	6.337	0.107	6.251	0.193
88c^t	6.143	6.135	0.008	6.151	-0.008
89c	6.444	6.673	-0.229	6.064	0.380
90c	6.602	6.736	-0.134	6.638	-0.036
91c^t	6.036	6.117	-0.081	6.581	-0.545
92c	6.301	6.701	-0.400	6.124	0.177

^{t}Test set.

Table **3**. The q^2, r^2_{cv}, r^2_{pred}, r^2_{ncv}, F and SEE values were computed as defined in SYBYL. PLS analysis showed a q^2 value of 0.613 and r^2_{cv} of 0.617. A non-cross-validated PLS analysis results in a conventional r^2_{ncv} of 0.886, F = 142 and a standard error of estimation (SEE) of 0.276 with 4 components. In both steric and electrostatic field contributions, former accounts for 0.537, while latter contributes 0.463, indicating that steric field contributed highest to the binding affinity. A total number of 4320 CoMFA field descriptors (electrostatic and steric each 2160) were calculated as independent variable, after a column filtering of 2.0 kcal/mol; 1722 CoMFA descriptors were used in the model generation study. A high boot strapped r^2 (0.846) value and low standard deviation (0.065) suggested a high degree of confidence in the analysis. The predicted, experimental pIC$_{50}$ and residual values are listed in Table **2**, and the correlation between the predicted and the experimental pIC$_{50}$ of training and test set is depicted in Fig. (**3**).
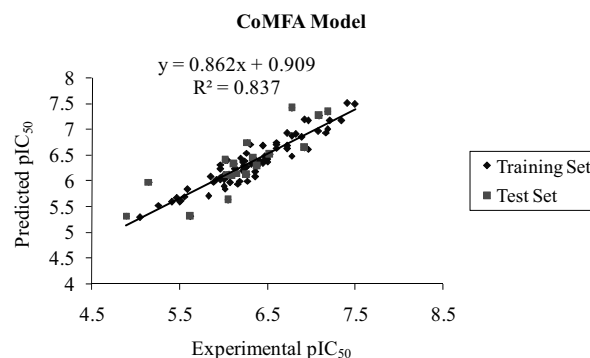

Fig. (3). Plot of experimental versus predicted pIC$_{50}$ of training and test set using CoMFA model.

3.2. Results of CoMSIA Study

CoMSIA offered steric, electrostatic, hydrophobic, hydrogen bond donor and acceptor field information. These

three additional factors in combination with steric and electrostatic fields resulted in best CoMSIA models. For the CoMSIA model, highest cross-validated q^2 and r^2_{cv} values were obtained by using the combination of steric, electrostatic, hydrophobic, H-bond donor and H-bond acceptor fields ($q^2 = 0.622$, $r^2_{cv} = 0.607$ $r^2_{ncv} = 0.859$, $F = 120$, SEE = 0.134) with 4 components. The corresponding field contribution is 0.153, 0.189, 0.207, 0.201 and 0.250, respectively. A total number of 10800 CoMSIA field descriptors (electrostatic, steric, hydrophobic, HBD and HBA each 2160) were calculated as independent variable, after a column filtering of 2.0 kcal/mol, 9627 CoMSIA descriptors were used in the model generation study. CoMSIA analysis results are summarized in Table **3**. The correlation between predicted and experimental activity of training and test set is depicted in Fig. (**4**).

Table 3.   Statistical Parameters of CoMFA and CoMSIA Model by PLS Analysis

Statistical Parameters	CoMFA Model	CoMSIA Model
N	4	4
q^2	0.613	0.622
r^2_{cv}	0.617	0.607
r^2_{ncv}	0.886	0.859
r^2_{pred}	0.714	0.549
Probability of r^2_{ncv}	0.000	0.000
SEE	0.276	0.134
F_{test}	142	120
r^2_{boot}	0.846	0.861
SEE$_{boot}$	0.131	0.075
SD$_{bs}$	0.065	0.014
Contributions		
Steric	0.537	0.153
Electrostatic	0.463	0.189
Hydrophobic	-	0.207
Hydrogen bond donor	-	0.201
Hydrogen bond acceptor	-	0.250

N is the optimal number of components (PLS components), q^2 is the leave-one-out (LOO) corelation coefficient, r^2_{cv} is cross-validation coefficient, r^2_{ncv} is the non-cross-validation coefficient, r^2_{pred} is the predictive correlation coefficient, SEE is the standard error of estimation, F is the F-test value, r^2_{bs} is mean r^2 of boot strapping analysis (100 runs), SD$_{bs}$ is mean standard deviation by bootstrapping analysis.

3.3. Predictive Power of the 3D QSAR Models

The predictive abilities of the 3D QSAR models were validated using a test set of 18 compounds, which was not included in the model generation study. The predicted r^2 (r^2_{pred}) values of CoMFA and CoMSIA models were 0.714 and 0.549, respectively (Table **3**). The 3D QSAR models were further validated by prediction of pIC$_{50}$ values using an external dataset of 10 substituted benzimidazole compounds as ARBs. A non-cross-validated PLS analysis resulted in a conventional r^2 of 0.893 for COMFA model and 0.774 for CoMSIA model. Table **4** summarized the predicted results

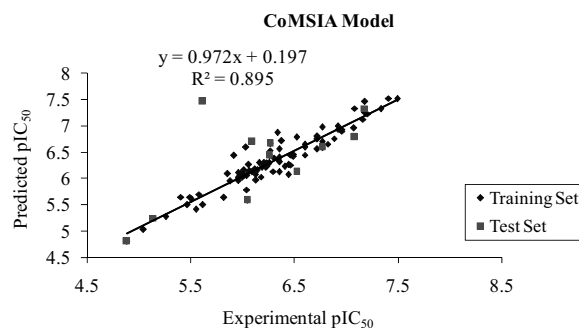obtained from the CoMFA and CoMSIA models for an external data set.

Fig. (4). Plot of experimental versus predicted pIC$_{50}$ of training and test set using CoMSIA model.

3.4. CoMFA Contour Maps

The contour maps of CoMFA denote the region in the space where aligned molecules would favourably or unfavourably interact with AT$_1$ receptor binding site. Steric and electrostatic field contributions account for 0.537 and 0.463 respectively, indicating that these two factors nearly contributed same to the binding affinity. Contour maps for the best CoMFA model are shown in Fig. (**5**). In the contour maps, the steric CoMFA contour plot of the most active compound **55b** is shown in Fig. (**5a**). The field energies at each lattice point were calculated as the scalar results of the coefficient and the standard deviation associated with a particular column of the data table (std*coeff), as always plotted as the percentages of the contribution of CoMFA equation. In this figure, green (G) contour represents the region of high steric tolerance, while yellow (Y) contour represent the region of low steric bulk tolerance. The steric contour of CoMFA model showed a large green contour near the first phenyl ring of the biphenyl ring template and covering the methylene linker between benzimidazole and biphenyl ring, indicated that sterically bulky groups are favored in this region. A second favorable steric contour was found near the second phenyl ring of the biphenyl ring system. Biphenyl ring system helped to occupy hydrophobic cavity in the active site of AT$_1$ receptor. Most of the active compound of the data set extended their bulky substitution (biphenyl ring) into the sterically favored green contour map of CoMFA and therefore exhibited good antagonistic activity. A third small green contour was present in the region of C2- position (–MeO) of benzimidazole ring. Compound **41b** (IC$_{50}$= 0.46 X 10^{-7}M) showed better activity due to the presence of –Et group at C2- position of benzimidazole ring, whereas **40b** (IC$_{50}$= 1.9 X 10^{-7}M) contains –Me group at this position, which is less hydrophobic than –Et, thus showing decrease in activity. One steric unfavorable yellow (Y) contour was observed near C7- (–COOH) and C6- position of benzimidazole ring, which suggested that bulky group in these regions would decrease AngII antagonistic activity. For example, compound **20b** (IC$_{50}$= 13 X 10^{-7}M) contained methyl group at C5-position, exhibited less activity as compared to other compounds having unsubstituted C5-position, such as **34b**

Table 4.   **Structure, Experimental and Predictive pIC$_{50}$ Values with Residuals of External Validation Compounds Using CoMFA and CoMSIA Models**

Compound	R	XH	Experimental pIC$_{50}$	CoMFA Model		CoMSIA Model	
				Predicted pIC$_{50}$	Residuals	Predicted pIC$_{50}$	Residuals
1	CH$_3$(CH$_2$)$_4$NH	COOH	6.409	6.442	0.033	6.582	0.173
2	CH$_3$(CH$_2$)$_3$-CONH	COOH	7.066	7.053	-0.013	7.084	0.018
3	(CH$_3$)$_2$NCONH	COOH	7.620	7.486	-0.134	7.445	-0.175
4	C$_6$H$_{11}$NHCO-NCH$_3$	COOH	7.585	7.262	-0.323	7.119	-0.466
5	CH$_3$(CH$_2$)$_2$SO$_2$-NCH$_3$	COOH	7.481	7.219	-0.262	7.838	0.357
6	C$_6$H$_{11}$NHCONH	Tetrazole	7.678	7.552	-0.126	7.662	-0.016
7	C$_6$H$_{11}$NHCONCH$_3$	Tetrazole	8.000	7.658	-0.342	8.561	0.561
8	(CH$_3$)$_2$NCONH	Tetrazole	8.097	8.264	0.167	8.020	-0.077
9	(piperidine structure)	COOH	6.796	6.760	-0.036	6.751	-0.045
10	(sultam structure)	COOH	7.469	7.536	0.067	7.675	0.206

(IC$_{50}$= 1.9 X 10^{-7}M). The reason being, **34b** has electropositive hydrogen atom filling yellow contour space.

In the CoMFA electrostatic contour map, regions where increased positive-charge is favorable for antagonistic activity are indicated in blue (B) contour, while regions where increased negative charge is favorable for antagonistic activity are indicated in red (R) contour. The electrostatic contour map is shown in Fig. (**5b**), which displayed one red contour close to terminal phenyl ring of biphenyl ring system, which suggested that electronegative groups such as –Cl, –F and –NO$_2$ at this position would increase the antagonistic activity as compared to hydrogen atom. A large blue contour was observed around the first phenyl ring of the biphenyl ring, which was covering tetrazole ring, indicated that a positively charged group at this position would increase the activity. Addition of positively charged substituents (*t*-Bu, allyl) at the first phenyl ring is preferred for the antagonistic activity. However, the present series of compounds do not contain any substitution at this position. A second blue contour was covering the linker –CH$_2$ between benzimidazole and biphenyl ring. The blue contour depicted that electropositive –CH$_2$ linker is required to show better activity.

3.5. CoMSIA Contour Maps

The CoMSIA contour maps denote those areas within the specified region where the presence of a group with a particular physicochemical property will be favoured or disfavoured for good antagonistic activity. The advantage of CoMSIA contour maps over CoMFA is that they are easy to interpret. CoMSIA calculates both steric and electrostatic fields, as in CoMFA, but additionally uses hydrophobic, hydrogen-bond donor and acceptor fields. The CoMSIA steric and electrostatic PLS contour maps were similarly placed as those of the CoMFA model. The contour plots of the CoMSIA hydrophobic, H-bond acceptor (HBA) and H-bond donor (HBD) fields (std*coeff) are shown in Fig. (**6**). The most active compound **55b** is overlaid in the maps once again. Fig. (**6a**) showed the hydrophobic plot represented by yellow (Y) and grey (Gr) contours. Yellow contours indicate regions where hydrophobic groups on ligands are favored and grey contours represent areas where hydrophobic groups are unfavored (or favorable for hydrophilic groups on ligands). Table **3** showed that hydrophobic field made the second largest contribution to the CoMSIA models. In the CoMSIA hydrophobic map, one large yellow contour was distributed under biphenyl ring system, near –MeO side
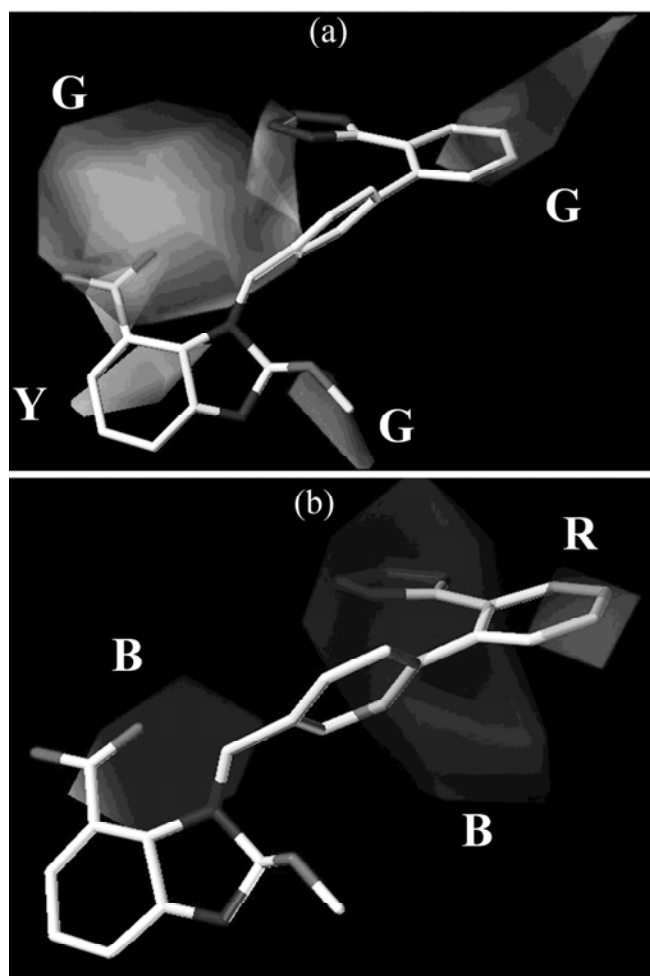
Fig. (5). CoMFA (std*coeff) contour maps. Compound **55b** is shown inside the field, (**a**) contour maps of CoMFA steric map is shown in green (G) contour refers to sterically favored regions; yellow (Y) contour indicated disfavored area, (**b**) contour map of CoMFA electrostatic field. Electrostatic contour map is shown in red (R) contour indicated region where negatively charged substituents are favored and blue (B) contour refers to regions where negatively charged substituents are disfavored.

chain and imidazole –N atom of benzimidazole ring, which indicated that hydrophobic groups in this area are beneficial to enhance antagonistic activity. The hydrophobic favored regions around the biphenyl ring and methoxy side chain were similarly placed as the steric favored regions in steric contour map. Presence of lipophilic group at R_2 position in **42b** (IC_{50} = 1.7 X 10^{-7}M) and **43b** (IC_{50} = 0.82 X 10^{-7}M) showed better activity. One grey contour near the C6-positon of benzimidazole ring revealed the necessity of the hydrophilic groups to increase the activity. For example, molecule **5a** (IC_{50}= 31 X 10^{-7}M) containing –Cl group at C6-position, exhibited less activity as compared to compounds **1a** (IC_{50} = 9 X 10^{-7}M). There is no such electronegative substitution in **1a**, hence it showed good activity. Second small grey contour was observed near –N atoms of tetrazole ring. Difference in the activity of **25a** and **26a** (**25a**: IC_{50}= 34 X 10^{-7}M; **26**: IC_{50}= 5.4 X 10^{-7}M) was due to the presence of more sterically favoured methyl group substituted at tetrazole ring in **25a**, where as **26a** do not contain methyl group at this position. Hydrophobic unfavored grey contour

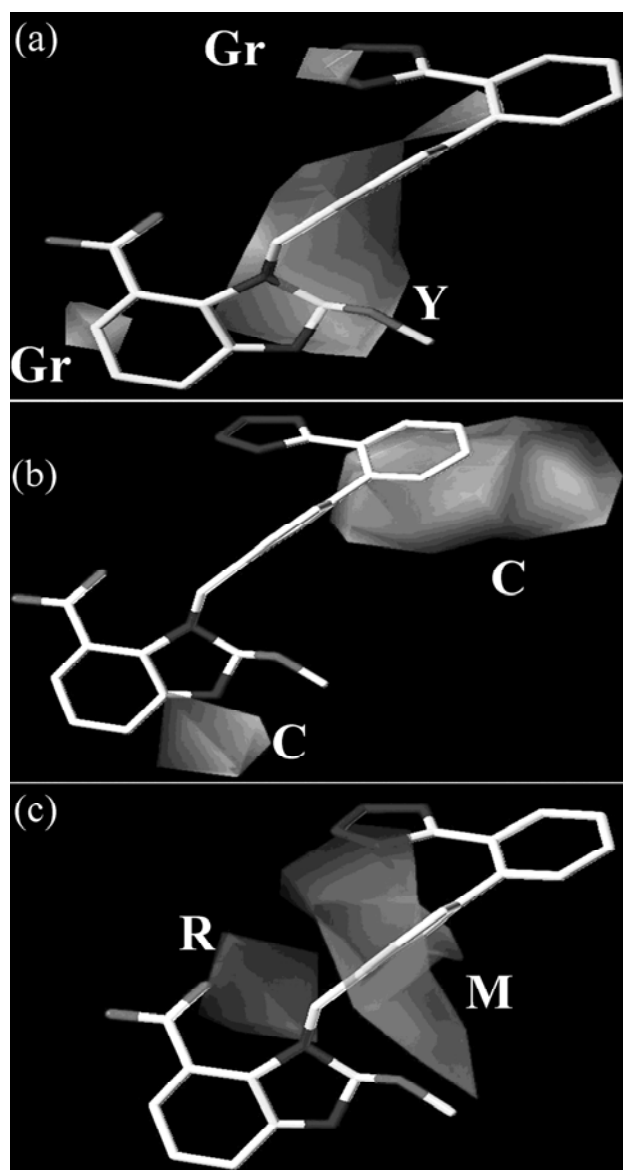is in agreement with sterically unfavored yellow color contour.

Fig. (6). CoMSIA (std*coeff) contour maps. Compound **55b** is shown inside the field, (**a**) Hydrophobic field, (**b**) HBD field, and (**c**) HBA field. Yellow (Y) and grey (Gr) contours indicate regions where hydrophobic groups favored and disfavored the activity, respectively. Cyan (C) contour represent areas where HBD favored. Magenta (M) and red (R) contours represent areas where HBA favored and disfavored, respectively.

The graphical interpretation of the hydrogen-bond donor (HBD) interactions in the CoMSIA model is represented in Fig. (**6b**). Cyan (C) contours indicated regions where HBD substituents on ligands are favored. In the HBD contour map two cyan areas were observed; one is near –N atom of benzimidazole ring and second cyan contour was found near terminal phenyl ring of biphenyl ring system. Nitrogen atom is necessary for a cyan favorable isopleth in proximity to this area. Nitrogen atom in benzimidazole ring usually can form H-bond with amino acid residues of the binding site of AT_1 receptor. The graphical interpretation of the hydrogen-bond
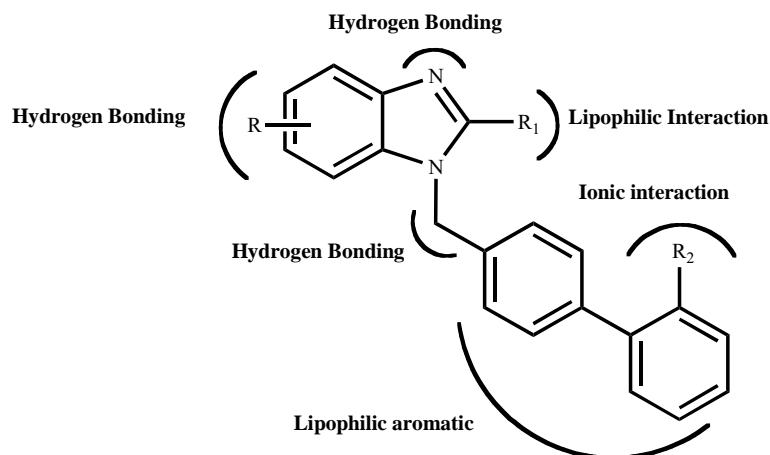
Fig. (7). Substituted benzimidazole derivatives–AT$_1$ receptor binding site interactions (Hypothetical model).

acceptor (HBA) interactions in the CoMSIA model is shown in Fig. (**6c**). Magenta (M) and red (R) contours represent areas where HBA are favored and disfavored, respectively. Table **3** showed that HBA made largest contribution to CoMSIA model. A large magenta contour was present near the first phenyl ring, which was also covering the tetrazole ring substituted on terminal phenyl ring of biphenyl ring system. Presence of magenta contour indicated that HBA groups in this region would increase the activity. HBA unfavoured red region was observed near carbonyl oxygen of C7-carboxylic acid, which means that HBA groups in this region would decrease antagonistic activity. Analysis of CoMFA and CoMSIA contour plots offered enough information to understand the binding mode between the ARB$_s$ and binding site of AT$_1$ receptor.

3.6. Substituted Benzimidazole Derivatives–AT$_1$ Receptor Binding Site Interaction (Hypothetical Model)

Substituted benzimidazole derivatives as AngII-AT$_1$ receptor antagonist appear to provide an opportunity as better therapeutic agents for the treatment of hypertension. Based upon various experimental findings discussed above, common steric, electrostatic, hydrophobic, and hydrogen bonding properties of substituted benzimidazole derivatives for the AT$_1$ receptor binding site are displayed in Fig. (**7**).

Several structural features necessary for AT$_1$ receptor binding affinity are (1): alkyl and alkoxy groups (*n*-Bu/*n*-Pr/MeO/EtO) at the C2- of benzimidazole ring, considered to be essential groups for lipophilic van der Waals interactions with the binding site; (2): ionized acidic group (tetrazole/carboxyl) on biphenyl ring template is responsible for ionic interaction with AT$_1$ receptor site; (3) lone pair of electron on N-atom forms H-bond with AT$_1$ receptor site; (4) biphenyl ring system is responsible for aromatic hydrophobic interaction with AT$_1$ receptor; (5) Substitution variations at C5-,6- and 7- position of benzimidazole ring interacts with receptor pocket through van der Waal and/or H-bonding interactions.

4. CONCLUSIONS

Selective inhibition of AngII is an important strategy for design and synthesis of ARBs, which are devoid of the common side effects of ACEIs. With the above facts and in continuation of our research for newer ARBs, we reported 3D QSAR (CoMFA and CoMSIA) study. In the present study, good predictive CoMFA and CoMSIA models were developed, and used for the prediction of AngII-AT$_1$ receptor antagonistic activity of an external data set (substituted benzimidazole compounds). CoMFA and CoMSIA models were satisfactory according to the statistical results as well as the contour maps analysis. Overall, the predictive power of CoMFA model appeared to be better than that of CoMSIA model based on r^2_{pred} values. CoMFA and CoMSIA models discussed in this study will be exploited to design novel compounds as ARBs.

CONFLICT OF INTEREST

The authors confirm that this article content has no conflict of interest.

REFERENCES

[1]   Vallotton, M.B. The renin-angiotensin system. *Trends Pharmacol. Sci.*, **1987**, *8*, 69-74.
[2]   Zaid, A.; Winaver, J.; Feuerste, G.Z. The biochemical pharmacology of renin inhibitors: Implications for translational medicine in hypertension, diabetic nephropathy and heart failure: expectations and reality. *Biochem. Pharmacol.*, **2009**, *78*, 933-940.
[3]   Hall, J.E. Historical perspective of the renin-angiotensin system. *Mol. Biotechnol.*, **2003**, *24*, 27-39.
[4]   Reudelhuber, T.L. The renin-angiotensin system: peptides and enzymes beyond angiotensin II. *Curr. Opin. Nephrol. Hypertens.*, **2005**, *14*, 155-159.
[5]   Carey, R.M.; Siragy, H.M. Newly recognized components of the renin-angiotensin system: potential roles in cardiovascular and renal regulation. *Endocr. Rev.*, **2003**, *24*, 261-271.
[6]   Menard, J.; Bouhnik, J.; Clauser, E.; Richoux, J.P.; Corvol, P. Biochemistry and regulation of angiotensinogen. *Clin. Exp. Hypertens.*, **1983**, *445*, 1005-1019.
[7]   Persson, P.B.; Skalweit, A.; Thiele, B.J. Controlling the release and production of renin, *Acta. Physiol. Scand.*, **2004**, *181*, 375-381.
[8]   Ibrahim, M.M. RAS inhibition in hypertension. *J. Hum. Hypertens.*, **2006**, *20*, 101-108.

[9] Herblin, W.F.; Chiu, A.T.; McCall, D.E.; Ardecky, R.J.; Carini, D.J.; Duncia, J.V.; Pease, L.J.; Wong, P.C.; Wexler, R.R.; Johnson, A.L.; Timmermans, P.B.M.W.M. Angiotensin II receptor heterogeneity. *Am. J. Hypertens.,* **1991**, *4*, 2099-3028.

[10] Pagliaro, P.; Penna, C. Rethinking the renin-angiotensin system and its role in cardiovascular regulation. *Cardiovasc. Drugs Ther.*, **2005**, *19*, 77-87.

[11] McConnaughey, M.; McConnaughey, J.S.; Ingenito, A.J. Practical considerations of the pharmacology of angiotensin receptor blockers. *J. Clin. Pharmacol.,* **1999**, *39*, 547-59.

[12] Hollenberg, N.K.; Fisher, N.D.L.; Price, D.A. Pathways for angiotensin II generation in intact human tissue: evidence from comparative pharmacological interruption of the renin system. *Hypertension,* **1998**, *32*, 387-392.

[13] Peach, M.J.; Dostal, D.E. The angiotensin II receptor and the actions of angiotensin II. *J. Cardiovasc. Pharmacol.,* **1990**, *16*, S25-S30.

[14] Ferrario, C.M. Role of angiotensin II in cardiovascular disease-therapeutic implications of more than a century of research. *J. Renin Angiotensin Aldosterone Syst.*, **2006**, *7*, 3-14.

[15] Stanton, A. Therapeutic potential of renin inhibitors in the management of cardiovascular disorders. *Am. J. Cardiovasc. Drugs*, **2003**, *3*, 389-394.

[16] Tenenbaum, A.; Grossman, E.; Shemesh, J.F.; Isman, E.Z.N.; Osrati, I.; Motro, M. Intermediate but not low doses of aspirin can suppress angiotensin-converting enzyme inhibitor-induced cough. *Am. J. Hypertens.,* **2000**, *13*, 776-782.

[17] Nussberger, J.; Cugno, M.; Amstutz, C.; Cicardi, M.; Pellacani, A.; Agostoni, A. Plasma bradykinin in angio-oedema. *Lancet,* **1998**, *351,* 1693-1697.

[18] Carini, D.J.; Duncia, J.V.; Aldrich, P.E.; Chiu, A.T.; Johnson, A.L.; Pierce, M.E.; Price, W.A.; Snatella, J.B.; Wells, G.J.; Wexler, R.R.; Wong, P.C.; Yoo, S.E.; Timmermans, P.B.M.W.M. Nonpeptide angiotensin II receptor antagonist: the discovery of a series of N-{biphenyl methyl} imidazole as potent orally active antihypertensive. *J. Med. Chem.,* **1991**, *34*, 2525-2547.

[19] Kubo, K.; Yasuhisa, K.; Imamiya, E.; Yoshihiro, S.; Inada, Y.; Furukawa, Y.; Nishikawa, N.T. Nonpeptide angiotensin II receptor antagonist synthesis and biological activity of benzimidazole carboxylic acids. *J. Med. Chem.,* **1993**, 36, 2182-2195.

[20] Ries, U.J.; Mihm, G.; Narr, B.; Hasselbach, K.M.; Wittneben, H.; Entzeroth, M.; Van Meel, J.C.; Wienen, W.; Hauel, N.H. 6-Substituted benzimidazoles as new nonpeptide angiotensin II receptor antagonists: synthesis, biological activity, and structure activity relationships. *J. Med. Chem.,* **1993**, *25*, 4040-4051.

[21] Vyas, V.K.; Ghate, M. Substituted benzimidazole derivatives as angiotensin II-AT₁ receptor antagonist: A review. *Mini-Rev. Med. Chem.,* **2010**, *10*, 1366-1384.

[22] Sagardia, I.; Roa-Ureta, R.H.; Bald, C. A new QSAR model, for angiotensin I-converting enzyme inhibitory oligopeptides. *Food Chem.,* **2013**, *15*, 1370-1376

[23] He, R.; Ma, H.; Zhao, W.; Qu, W. Zhao J, Luo L, Zhu W. Modeling the QSAR of ACE-Inhibitory Peptides with ANN and Its Applied Illustration. *Int. J. Pept.,* **2012**, *2012* doi: 10.1155/2012/620609

[24] Shu, M.; Cheng, X.; Zhang, Y.; Wang, Y.; Lin, Y.; Wang, L.; Lin Z. Predicting the activity of ACE inhibitory peptides with a novel mode of pseudo amino acid composition. *Protein Pept. Lett.,* **2011**, *18*, 1233-1243.

[25] Wang, X.; Wang, J.; Lin, Y.; Ding, Y.; Wang, Y.; Cheng, X.; Lin Z. QSAR study on angiotensin-converting enzyme inhibitor oligopeptides based on a novel set of sequence information descriptors. *J. Mol. Model.,* **2011**, *17,*1599-1606.

[26] Ponce, Y.M.; Diaz, H.G.; Zaldivar, V.R.; Torrens, F.; Castro E.A. 3D-chiral quadratic indices of the 'molecular pseudograph's atom adjacency matrix' and their application to central chirality codification: classification of ACE inhibitors and prediction of sigma-receptor antagonist activities. *Bioorg. Med. Chem.*, **2004**, *15*, 5331-5342.

[27] Gupta, S.P. Quantitative structure-activity relationships of antihypertensiveagents. *Prog. Drug Res.*, **1999**, *53*, 53-87.

[28] Díaz, H.G.; Sánchez, I.H.; Uriarte, E.; Santana, L.; Symmetry considerations in Markovian chemicals 'in silico' design (MARCH-INSIDE) I: central chirality codification, classification of ACE inhibitors and prediction of sigma-receptor antagonist activities. *Comput. Biol. Chem.*, **2003**, *27*, 217-227.

[29] Castillo-Garit, J.A.; Marrero-Ponce, Y.; Torrens, F.; Rotondo, R. Atom-based stochastic and non-stochastic 3D-chiral bilinear indices and their applications to central chirality codification. *J. Mol. Graph. Model.*, **2007**, *26*, 32-47.

[30] Castillo-Garit, J.A.; Marrero-Ponce, Y.; Torrens, F.; García-Domenech, R.; Romero-Zaldivar, V. Bond-based 3D-chiral linear indices: theory and QSAR applications to central chirality codification. *J. Comput. Chem.*, **2008**, *30*, 2500-2512.

[31] Jain, A.; Chaturvedi, S.C.; QSAR modeling of some substituted benzimidazole as Angotensin II AT1 receptor antagonist. *Med. Chem. Res.*, **2010**, *19*, 177-185.

[32] Jain A.; Chaturvedi S.C. Rationalization of physicochemical property of some substituted benzimidazole bearing acidic heterocyclic towards angiotensin II antagonist: a QSAR approach. *Asian. J. Biochem.,* **2008**, *3*, 330-336.

[33] Jain, A.; Chaturvedi, S.C. QSAR study on 6-Substituted Benzimidazoles: An insight into the structural requirement for the angiotensin II AT1 receptor antagonist. *Sci. Pharm.,* **2009**, *77*, 555-565.

[34] Sharma, M.C.; Kohli, D.V. A comprehensive structure–activity analysis of 5-Carboxyl Imidazolyl biphenyl Sulfonylureas derivatives angiotensin AT1 receptor antagonists: 2D- and 3D-QSAR approach. *Arabian J. Chem.*, **2012**, http://dx.doi.org/10.1016/j.arabjc.2012.04.020.

[35] Sharma, M.C.; Kohli, D.V. QSAR analysis and 3D QSAR kNN-MFA approach on a series of substituted quinolines derivatives as angiotensin II receptor antagonists. *Arabian J. Chem.,* **2011**, doi:10.1016/j.arabjc.2011.07.008.

[36] Sharma, M.C.; Kohli, D.V. QSAR studies on substituted benzi-midazoles as angiotensin II receptor antagonists: kNN-MFA approach. *Arabian J. Chem.*, **2011**, doi:10.1016/j.arabjc.2011.05.015.

[37] Sharma, M.C.; Kohli, D.V. Comprehensive structure–activity relationship analysis of substituted 5-(biphenyl-4-ylmethyl) pyrazoles derivatives as AT1 selective angiotensin II receptor antagonists: 2D and kNNMFA QSAR approach. *Med. Chem. Res.*, **2013**, *22*, 2124-2138.

[38] Sharma, M.C.; Kohli, D.V. A comprehensive structure–activity analysis 2,3,5-trisubstituted 4,5-dihydro-4-oxo-3*H*-imidazo [4,5-*c*] pyridine derivatives as angiotensin II receptor antagonists using 2D- and 3D-QSAR approach. *Med. Chem. Res.*, **2013**, *22*, 588-605.

[39] Sharma, M.C.; Kohli, D.V. Insight into the structural requirement of aryltriazolinone derivatives as angiotensin II AT1 receptor: 2D and 3D-QSAR k-nearest neighbor molecular field analysis approach. *Med. Chem. Res*., **2012**, *21*, 283-2853.

[40] Sharma, M.C.; Kohli, D.V. Comprehensive two and three-dimensional QSAR studies of 3-substituted 6-butyl-1,2dihydropyridin-2-ones derivatives as angiotensin II receptor antagonists. *Med. Chem. Res.*, **2013**, *22*, 1107-1123.

[41] Vyas, V.K.; Ghate, M.D.; QSAR modeling of substituted benzimidazole derivative as angiotensin II-AT1 receptor antagonist: WHIM descriptors *Int. J. Drug Des. Discov.*, **2011**, *2*, 375-382.

[42] Vyas, V.K.; Jain, A.; Mahajan, S.C.; Patidar, R.; Mistry, S.; Chaturvedi, S.C. Insight into the structural requirement of 2-Alkyl-4-(biphenylmethoxy)quinolines as nonpeptide angiotensin II receptor antagonists: A QSAR Approach. *Sci. Pharm.*, **2009**, *77*, 33-45.

[43] Vyas, V.K.; Ghate, M. CoMFA and CoMSIA studies on aryl carboxylic acid amide derivatives as dihydroorotate dehydrogenase (DHODH) inhibitors. *Curr. Comput Aided Drug Des.*, **2012**, *8*, 271-282.

[44] Verma, J.; Khedkar, V.M. 3D-QSAR in drug design - A review. *Cur. Top. Med. Chem.*, **2010**, *10,* 95-115.

[45] Klebe, G.; Abraham, U. Comparative molecular similarity index analysis (CoMSIA) to study hydrogen bonding properties and to score combinatorial libraries. *J. Comput. Aided Mol. Des.,* **1999**, *13,* 1-10.

[46] Kubo, K.; Yoshiyuki, I.; Yasuhisa, K.; Yoshihiro, S.; Mami, O.; Katsuhiko. I.; Yoshiyasu, F.; Kohei, N.; Takehiko, N. Nonpeptide angiotensin II receptor antagonist. Synthesis and biological activity of benzimidazole. *J. Med. Chem.*, **1993**, *36*, 1772-1784.

[47] Kohara, Y.; Kubo, K.; Imamiya, E.; Inada, Y.; Naka, T. Synthesis and angiotensin II receptor antagonistic activities of benzimidazole derivatives bearing acidic heterocycles as novel tetrazole bioisosteres. *J. Med. Chem.,* **1996**, *39*, 5228-5235.

[48]   Tripos Associates, SYBYL X Molecular Modeling Software, Version 1.2 (**2011**), St. Louis, MO, (http://www.tripos.com).

[49]   Gasteiger, J.; Marsili, M. Iterative partial equalization of orbital electronegativity- a rapid access to atomic charges. *Tetrahedron*, **1980**, *36*, 3219-3228.

[50]   Clark, M.; Cramer, R.D.; Opdenbosch, N.V. Validation of the general purpose Tripos 5.2 forcefield. *J. Comput. Chem.,* **1989**, *10*, 982-1012.

[51]   HCA^{TM} Manual, SYBYL X 1.2, Tripos, St. Louis, MO, **2011**.

[52]   Cramer III, R.D.; Bunce, J.D.; Patterson, D.E. Crossvalidation, bootstrapping, and partial least squares compared with multiple regression in conventional QSAR studies. *J. Am. Chem. Soc.,* **1988**, *110*, 5959-5967.

[53]   Hasegawa, K.; Funatsu K. Advanced PLS techniques in chemoinformatics studies*. Curr. Comput Aided Drug Des.,* **2010**, *6*, 103-127.